Preconditioning of the wintertime mixed layer at the Kuroshio Extension Observatory

Hiroyuki Tomita,[1] Shin'ichiro Kako,[2] Meghan F. Cronin,[3] and Masahisa Kubota[4]

[1] Summertime surface heat flux and upper ocean state in 2004, 2005, and 2006 obtained from the Kuroshio Extension Observatory (KEO) buoy were investigated, focusing on the summertime preconditioning of the following winter's mixed layer. Summertime net shortwave radiation at the surface shows large year-to-year variations that resulted in anomalous heating in 2005 and anomalous cooling in 2006. Covariation of the surface heat flux and upper ocean stratification was found and suggests that year-to-year variations of summertime heat flux induce corresponding changes in the near surface stratification. Cold core rings, observed in 2006, tend to intensify both the near surface (<100 m depth) density stratification and the density stratification below the seasonal thermocline (>100 m depth). Lateral and vertical heat fluxes evaluated from the imbalance between the observed heat storage rate and the net heat flux and entrainment also have a significant role in determination of upper ocean stratification and can intensify year-to-year variation of the mixed layer. The physical mechanism that determines the precondition of the next winter mixed layer can change each year. In 2005, near surface stratification induced by anomalous summertime heating has a dominant role compared to deeper stratification. On the other hand, in 2006, the much deeper stratification below the seasonal thermocline (>100 m depth) associated with cold core rings contributes to make the maximum vertical density stratification.

Citation: Tomita, H., S. Kako, M. F. Cronin, and M. Kubota (2010), Preconditioning of the wintertime mixed layer at the Kuroshio Extension Observatory, *J. Geophys. Res.*, *115*, C12053, doi:10.1029/2010JC006373.

1. Introduction

[2] It is well known that the Kuroshio and Kuroshio/Oyashio extension regions are characterized by large surface heat losses in wintertime which have a crucial role in the formation of mixed layer and subtropical mode water (STMW) [*Suga and Hanawa*, 1995a]. Several studies have indicated that the formation rate and properties of STMW show significant interannual and decadal variations related to changes in wintertime atmospheric forcing [*Suga and Hanawa*, 1995b]. On the other hand, *Qiu and Chen* [2006] have demonstrated that the formation of STMW and its subsequent evolution depends on the oceanic circulation conditions such as the preexisting density stratification and the level of mesoscale eddy activity at decadal time scale. Also, using a one-dimensional numerical model with surface flux derived from atmospheric reanalysis as surface boundary conditions, *Kako and Kubota* [2007] suggested that anomalous summertime surface fluxes enhance the seasonal thermocline beneath the mixed layer and can have an effect on the wintertime mixed layer. In order to verify their results and reveal the detailed processes of preconditioning, we examine in detail the processes responsible for year-to-year variations of summertime heat flux and their influence on the upper ocean stratification using in situ observations.

[3] In June 2004, the National Oceanic and Atmospheric Administration (NOAA) deployed the Kuroshio Extension Observatory (KEO) buoy in the Kuroshio Extension recirculation gyre [*Cronin et al.*, 2008]. The KEO buoy provided relatively long, continuous, high-quality time series of air-sea heat flux and upper ocean temperature/salinity. In the present study, we analyze the year-to-year variations of summertime heat flux and upper ocean stratification in 2004, 2005, and 2006 observed at KEO buoy. Data and method are described in section 2. Results are presented in section 3. The summary and discussion are given in section 4.

2. Data and Method

[4] The KEO buoy carries sensors to measure surface meteorological parameters and upper ocean temperature, salinity (conductivity) and pressure to 525 m. Table 1 summarizes oceanic sensor arrangement of each observation phase of the KEO buoy. Because the mooring of the KEO

[1]Research Institute for Global Change, Japan Agency for Marine and Earth Science Technology, Kanagawa, Japan.
[2]Center for Marine Environmental Studies, Ehime University, Matsuyama, Japan.
[3]NOAA Pacific Marine Environmental Laboratory, Seattle, Washington, USA.
[4]School of Marine Science and Technology, Tokai University, Shizuoka, Japan.

Table 1. Oceanic Sensor Arrange of the KEO Buoy[a]

	Sensor Type		
Wire Length, m	KEO-1	KEO-2	KEO-3
1	TC	TC	TC
5	TC	TC	TC
10/8.3	TC	TC/ V	TC/ V
15		TC	TC
18.3/17		T/ V	T/ V
25	TC	TC	TC
35		TC	TC
38.3/37		T/ V	T/ V
50	TC	TC	TC
75	TC	TC	TC
100	TP	TP	TP
125		TC	TC
150	TC	TC	TC
175		TP	TP
200	TC	TC	TC
225		T	T
250		TP	TP
275		TC	TC
300	TP	TP	TP
325		TC	TC
350		T	T
375		TP	TP
400	TC	TC	TC
425		TP	TP
450		T	T
475		TC	TC
500	TP	TP	TP
525		TC	TC

[a]T, C, P, and V mean sensor of temperature, conductivity, pressure, and current velocity, respectively. Oceanic sensor arrange is different depending on each observation phase, KEO-1 (from June 2004 to June 2005), KEO-2 (from June 2005 to November 2005), and KEO-3 (from May 2006 to May 2007).

buoy is a slack line with scope 1.4, the sensors can rise when the wire stretches out as it does under strong currents. Consequently, the sensor depths are variable and must be determined from the pressure measurements.

[5] Daily means of surface heat fluxes are calculated from high-resolution (10 min sampled) delayed-mode surface meteorological and oceanic parameters following the method described by *Kubota et al.* [2008]. It should be noted that a surface heat flux from the atmosphere to the ocean (i.e., downward surface heat flux) is defined to have a positive sign in this study. The daily mean delayed-mode data are also used to examine the upper ocean state. We calculated mixed layer depth as the depth at which the value of potential density differs from that at the sea surface by 0.125 kg/m^3.

[6] Unfortunately, the KEO buoy did not provide complete time series due to breaks in the mooring line. To extend the analysis through these gaps in the KEO data, we used a gridded monthly data set of temperature and salinity obtained from Argo floats and available conductivity-temperature-depth (CTD) named as the Grid Point Value of the Monthly Objective Analysis (MOAA GPV) using Argo float data [*Hosoda et al.*, 2008]. The MOAA GPV data provides monthly temperature and salinity data for the period 1999 to present on the 1° by 1° grids of the world oceans. We used data at the grid point of the KEO buoy. The distance between the center of grid and the buoy is roughly <50 km. It should be noted that CTD data obtained from the KEO buoy are not used in the MOAA GPV data. Although the information about number of profiles used in the objective

analysis in MOAA GPV was not provided, in general, there are relatively large number of Argo profiles over the western North Pacific, in particular after 2004 [*Hosoda et al.*, 2008].

[7] In addition, the version 2 of Japanese Ocean Flux data set with use of Remote sensing Observations (J-OFURO2) is used. Daily mean data at the KEO buoy is used to investigate long time series to support gaps in time series of KEO. In addition, daily mean data over the Kuroshio Extension region were used to investigate spatial pattern of summertime surface heat flux. The accuracy of the J-OFURO2 was assessed at the KEO/JKEO buoys [*Tomita et al.*, 2010]. They have shown that accuracy of J-OFURO2 is quite good compared with other global heat flux data sets (e.g., reanalysis), having a total bias and RMS errors of less than 10 and 60 W/m^2, respectively.

[8] Cloud liquid water (CLW) derived from satellite microwave radiometer observations were used to investigate spatial patterns of cloud and their relationship with incoming shortwave radiation. For this purpose, the daily means were constructed on the 0.25° by 0.25° grids over the global ocean using data from multiple satellites (DMSP SSMIs F13, 14, and 15), Aqua AMSR-E, and TRMM TMI.

[9] The Ocean Surface Current Analyses -Real Time (OSCAR) [*Bonjean and Lagerloef*, 2002] data were used for estimation of surface current and eddy kinetic energy (EKE) at the KEO site. OSCAR current data are constructed using surface height from satellite altimeter and surface vector wind speed obtained from satellite scatterometer. OSCAR currents have a 5 day sample rate on the 1° by 1° grid and are available in near realtime. Finally, sea surface dynamic height anomaly (SSHA) data from Archiving, Validation and Interpretation of Satellite Oceanographic data (Aviso) were also used to identify the spatial distribution of ocean topography.

[10] Best track data archived in Joint Typhoon Warning Center (JTWC) were used to detect route and period of tropical cyclone (TC) near KEO. The data contain location of TC center, maximum wind speed, and minimum sea level

Table 2. Summary of Tropical Cyclones Selected in This Study

| Year	Annual Cyclone Number	Name	Period	Max Wind (knt)
2004	11	TINGTING	2004/06/25–2004/07/02	80
	13	NAMTHEUN	2004/07/25–2004/08/01	115
	18	MEGI	2004/08/14–2004/08/19	65
	19	CHABA	2004/08/18–2004/08/31	155
	22	SONGDA	2004/08/27–2004/09/07	130
	25	MEARI	2004/09/20–2004/09/29	120
	26	MA-ON	2004/10/04–2004/10/09	140
	27	TOKAGE	2004/10/12–2004/10/20	125
2005	7	BANYAN	2005/07/21–2005/07/27	60
	11	MAWAR	2005/08/19–2005/08/26	130
	12	GUCHOL	2005/08/20–2005/08/25	60
	14	NABI	2005/08/29–2005/09/06	140
	18	SAOLA	2005/09/20–2005/09/26	90
	21	KIROGI	2005/10/10–2005/10/19	125
2006	4	EWINIAR	2006/06/29–2006/07/11	130
	9	MARIA	2006/08/05–2006/08/11	65
	11	WUKONG	2006/08/12–2006/08/20	50
	14	SHANSHAN	2006/09/10–2006/09/20	120
	16	YAGI	2006/09/17–2006/09/25	140
	21	SOULIK	2006/10/09–2006/10/16	90

(a) 2004
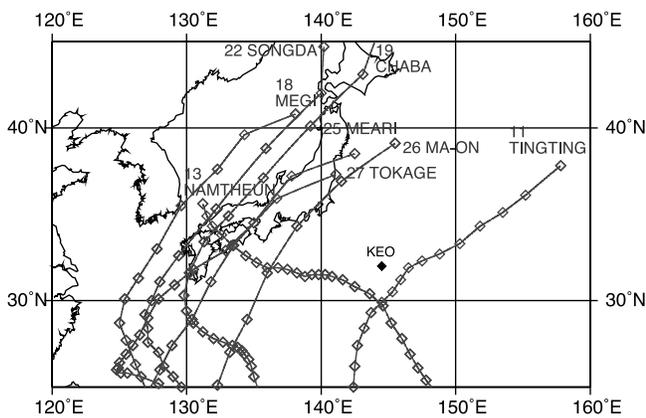
(b) 2005
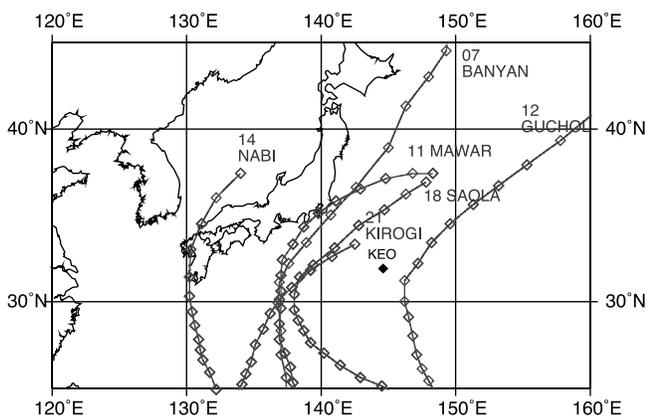
(c) 2006
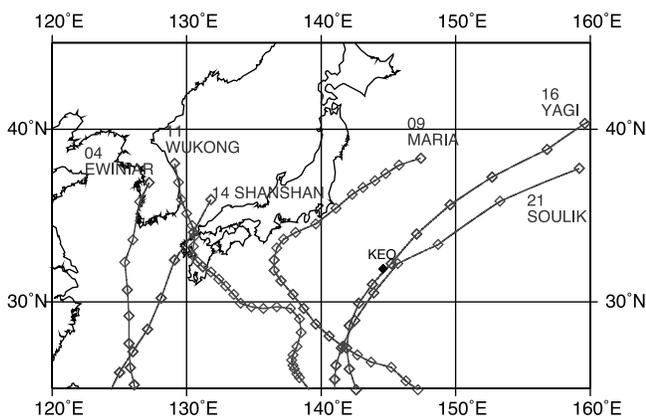
Figure 1. Locations of KEO and center of TC for each summer in (a) 2004, (b) 2005, and (c) 2006.

pressure. We selected TCs that met the following conditions: (1) TC center is in the region (125°E–155°E, 25°N–50°N), (2) in the period of 1 July–31 October, (3) maximum wind speed is over 34 knots, and (4) data number is greater

than 5. As a result, eight for 2004, six for 2005, and six for 2006 TCs were detected (see Figure 1 and Table 2).

[11] In this study, summertime is defined as 15 July to 15 October and wintertime is defined as 1 December to 28 February. Since there are no KEO observational data in winter 2005–2006 and 2006–2007, summertime mean are computed using KEO data, while wintertime mean are computed using only Argo MOAA GPV and J-OFURO2 data.

[12] In order to display overall features of observed air-sea heat flux and upper-ocean state, Figure 2 shows daily time series of air-sea net heat flux, temperature, and mixed layer depth from the KEO buoy. Since there are no KEO observational data during winters 2005–2006 and 2006–2007, we use J-OFURO2 and Argo MOAA GPV data at the KEO buoy (Figure 2b). Although temporal resolution of the Argo MOAA GPV data is quite a bit coarser compared with that of the KEO buoy data, the Argo MOAA GPV provides us with continuous oceanic temperature and salinity data. The brief comparison of temperature and mixed layer depth between the KEO and Argo MOAA GPV shows that seasonal and year-to-year variations from both data are quite similar. Therefore we can reasonably investigate influence of the oceanic precondition induced by summertime surface heat flux and oceanic variation on wintertime mixed layer using the MOAA GPV data.

3. Results

3.1. Observed Air-Sea Heat Flux and Upper-Ocean Variation at the KEO

[13] As mentioned in section 1, several studies have indicated that mixed layer changes covary with wintertime atmospheric forcing (i.e., air-sea flux) at interannual and decadal time scales. Comparison between wintertime air-sea heat flux and mixed layer depth show that there is little relationship between both (see Figure 2). For example, in winter 2005–2006, although there is the largest air-sea heat flux, mixed layer depth is relatively shallower. Also, although air-sea heat flux is almost the same in winters 2004–2005 and 2006–2007, mixed layer depths are quite different between both winters. The present study suggests that it is summertime preconditioning that is important for the evolution of the mixed layer in winter at KEO. As shown in Figure 2a, the KEO observations reveal high-frequency variation of air-sea flux and upper ocean state. In section 3.2, using the KEO buoy data, we investigate the processes of preconditioning of wintertime mixed layer in detail.

3.2. Year-to-Year Variation of Air-Sea Flux

[14] Mean and anomalous summertime heat fluxes computed from the KEO buoy measurements for 2004–2006 are shown in Table 3. Mean net heat flux is 84.4 W/m^2 into the ocean. This heating results from an imbalance between the large heating from shortwave radiation (224.7 W/m^2) and cooling from latent heat flux (−85.2 W/m^2) and net long-wave radiation (−49.3 W/m^2). The contribution of sensible heat flux is very small (−5.5 W/m^2). Net heat flux shows significant year-to-year variation, with slight heating (+6.5 W/m^2) in 2004, anomalous heating (+16.5 W/m^2) in 2005, and anomalous cooling (−22.9 W/m^2) in 2006. Both the anomalous heating in 2005 and cooling in 2006 are
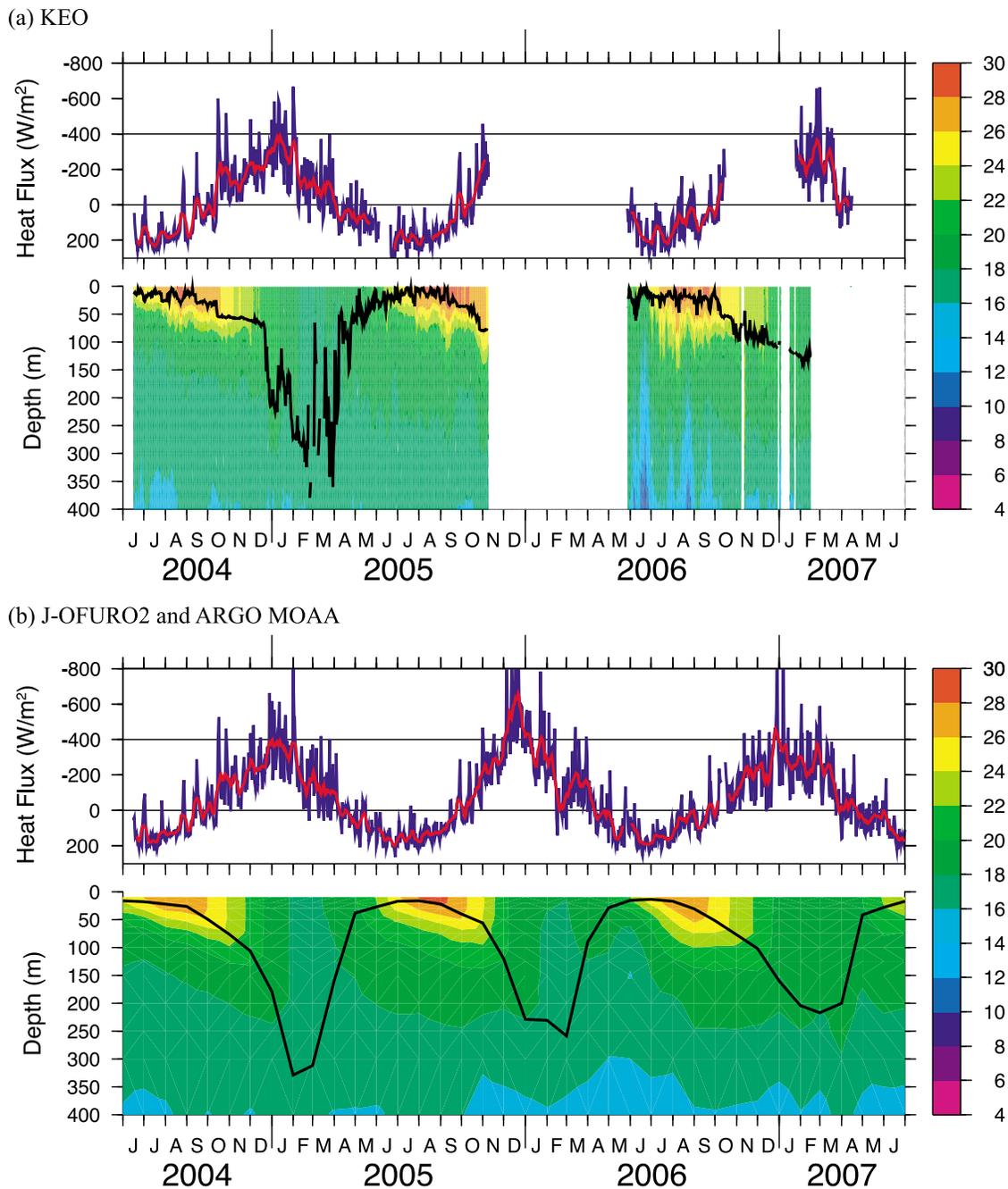
Figure 2. Time series of daily (upper: blue) and 10-day running mean (upper: red) of air-sea net heat flux (W/m^2) and mixed layer depth (lower: line, m) and temperature (lower: color, °C) obtained from (a) KEO buoy and (b) J-OFURO2 and Argo MOAA. Positive (negative) air-sea heat flux value means downward (upward) flux.

caused by variation of shortwave radiation, while the variations in the other heat fluxes are quite small (<5 W/m^2).

[15] In order to investigate why the incoming shortwave radiation is large (small) in 2005 (2006), in Figure 3 we show the daily variations of surface heat fluxes at KEO for each summer. The tropical cyclone periods defined by JTWC best track data are highlighted in Figure 3 and show that in many cases low incoming shortwave radiation (<200 W/m^2, i.e., a reduction of 200–250 W/m^2) lasting several days can be associated with tropical cyclones in the

proximity of the KEO buoy. Note that the frequency of the tropical cyclones, and resulting reduction of incoming shortwave radiation, varies from year to year. The year 2005 had fewer and weaker decreases in incoming shortwave radiation compared with 2004 and 2006. In contrast, in 2006, there were many periods of low incoming shortwave radiation. Variability in the occurrence of TCs is also confirmed from the summertime standard deviations of incoming shortwave radiation in each year (62.0 W/m^2 for 2004, 57.0 W/m^2 for 2005, and 74.4 W/m^2 for 2006).

Table 3. Comparison of Anomaly From the Summertime Average During 2004–2006 in Summertime Air-Sea Fluxes[a]

Variable	Summertime Average	Anomaly		
		2004	2005	2006
NET	84.4	6.4	16.5	−22.9
SWR	224.7	3.0	20.6	−23.5
LWR	−49.3	−2.5	0.5	2.0
LHF	−85.2	3.4	−4.5	1.1
SHF	−5.5	2.2	0.2	−2.4
MF	0.07	−0.004	−0.010	0.014

[a]Net heat flux (NET), net shortwave radiation (SWR), net longwave radiation (LWR), latent heat flux (LHF), sensible heat flux (SHF) and momentum flux (MF). Units in W/m^2 for air-sea heat fluxes. Units in N/m^2 for momentum flux.

Table 4. Same as Table 3 but for J-OFURO2 Fluxes

Variable	Summertime Average	Anomaly		
		2004	2005	2006
NET	70.3	2.0	19.0	−20.9
SWR	225.2	7.5	4.1	−11.5
LWR	−57.3	−3.0	1.6	1.4
LHF	−97.6	−2.1	12.2	−10.1
SHF	−0.1	−0.3	1.4	−1.1

[16] In order to investigate the relationship between year-to-year variation of surface heat flux at KEO and basin-scale spatial patterns, we analyzed data obtained from the global surface heat flux product. To start, the same analysis as shown in Table 3 was performed with the global product, J-OFURO2 at the KEO (Table 4). Both the summertime mean and year-to-year variation of net heat flux in J-OFURO2 indicates much better agreement with KEO compared with other global products (e.g., NCEP/NCAR reanalysis). J-OFURO2 underestimates summertime mean of net heat flux by about 15 W/m^2. The largest portion of the bias is due to the overestimation of cooling by latent heat flux. Year-to-year variation of net heat flux in J-OFURO2 is quite similar to that of KEO data. The balance of surface heat flux, however, is somewhat different from KEO, which shows large year-to-year variation of incoming shortwave radiation as mentioned above. Meanwhile, surface heat fluxes from J-OFURO2 show year-to-year variation in both incoming shortwave radiation and latent heat flux and the relative importance of those fluxes to the year-to-year variation of net heat flux is comparable. Although the KEO buoy shows anomalous incoming shortwave radiation in 2005 (20.6 W/m^2), J-OFURO2 shows relatively small positive heating anomaly (4.1 W/m^2). This difference might be due to the coarse spatial resolution of J-OFURO2 incoming shortwave radiation that was interpolated onto the 1.0° by 1.0° grid from the original ISCCP 280 km grid. In fact, cloud liquid water data on 0.25° by 0.25° grids obtained from multisatellite microwave radiometer, which is independent of J-OFURO2 SWR, show year-to-year variation is consistent with that of SWR observed by KEO buoy.

[17] In order to investigate spatial pattern of incoming shortwave radiation and its year-to-year variation, in Figure 4
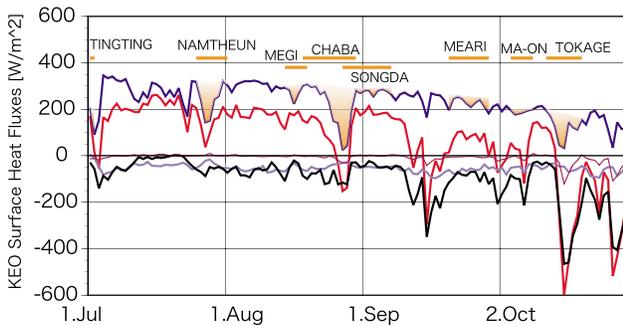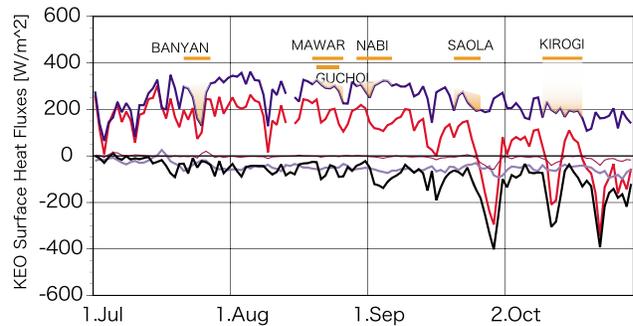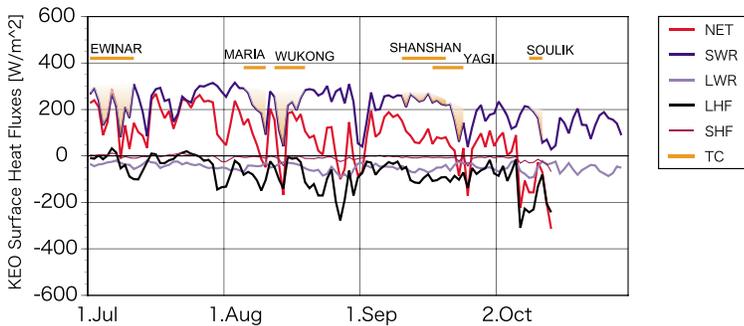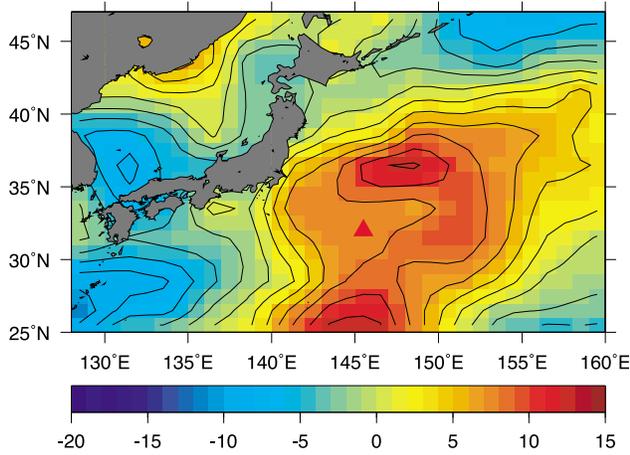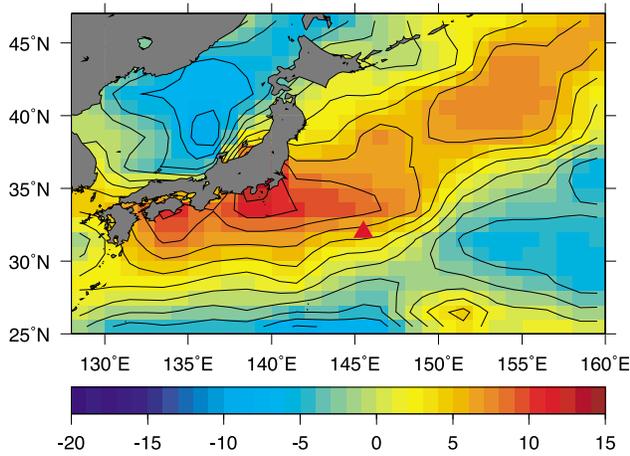

Figure 3. Time series of summertime surface heat fluxes at the KEO buoy in (a) 2004, (b) 2005, and (c) 2006. The periods of tropical cyclone is superimposed as orange line and shade.
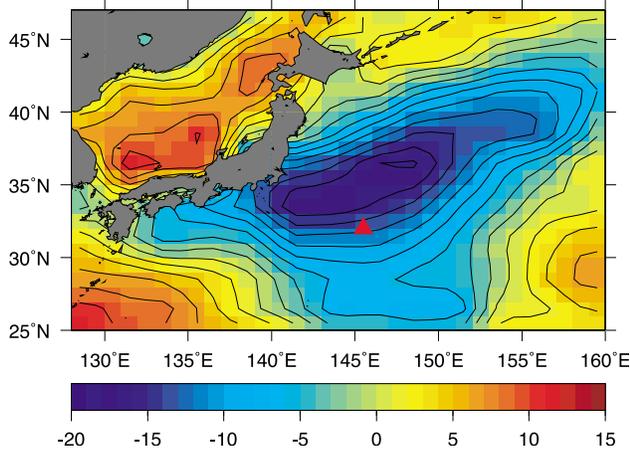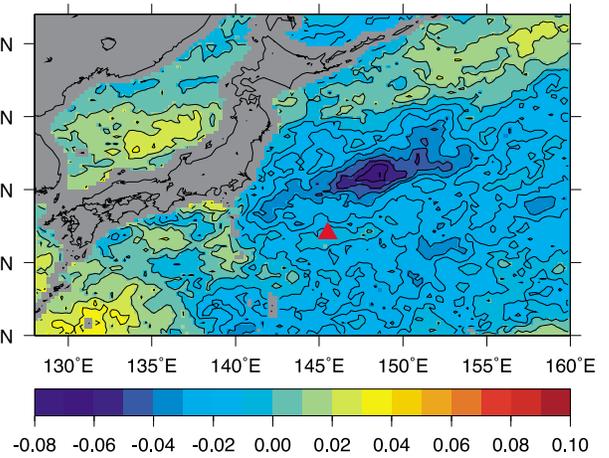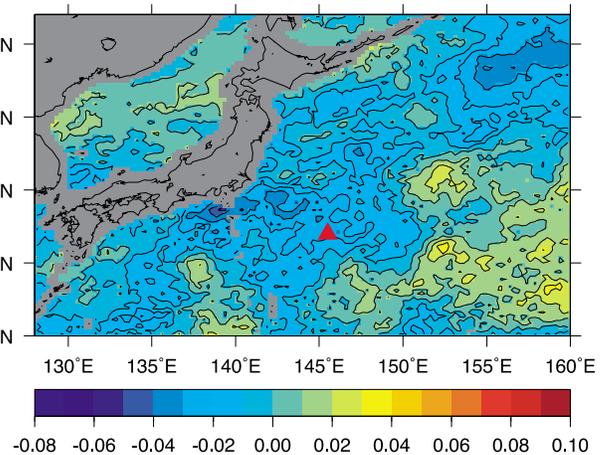
Figure 4. Spatial distribution of anomalous incoming shortwave radiation (W/m^2) obtained from J-OFURO2 for each summer in (a) 2004, (b) 2005, and (c) 2006. Red triangle shows KEO buoy location.
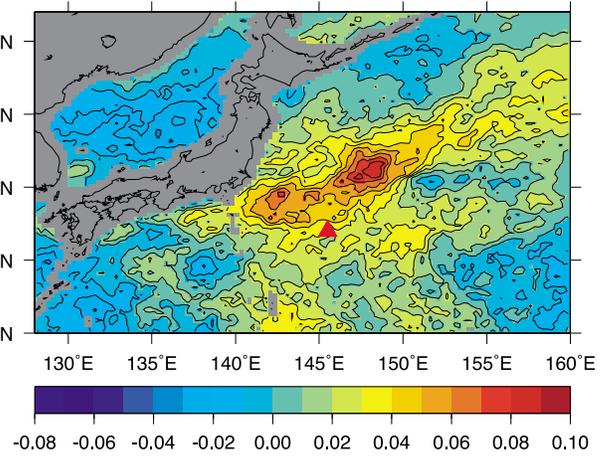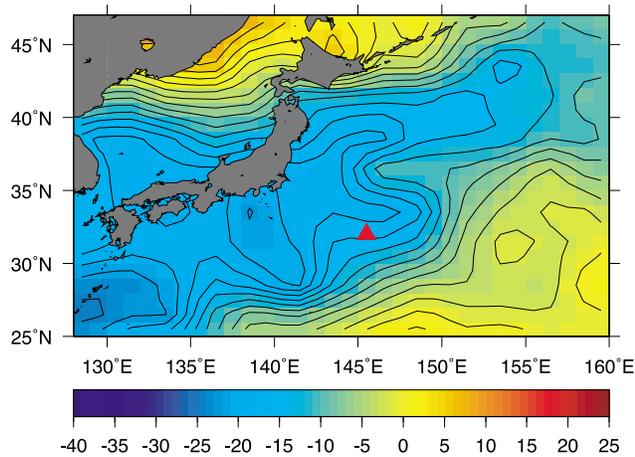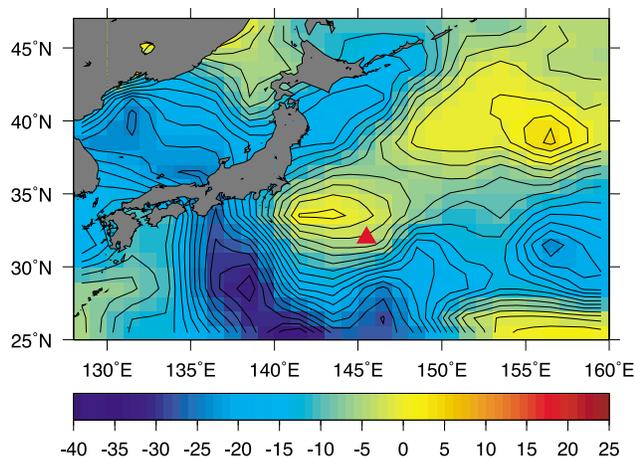

Figure 5. Same as Figure 4 but for cloud liquid water (mm) obtained from synthesis of multi microwave radiometers.
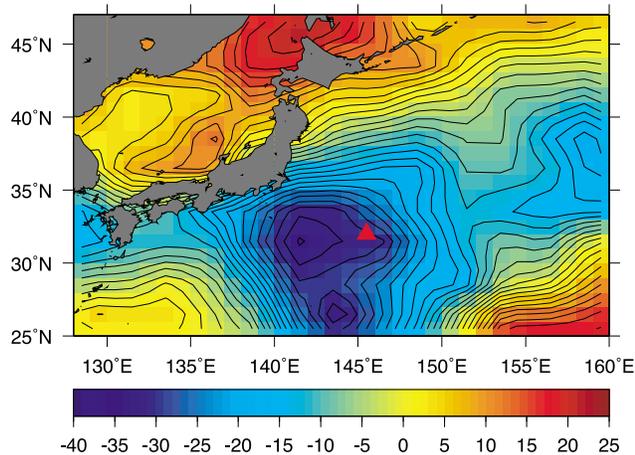
(a) 2004

(b) 2005

(c) 2006

we show the spatial distribution of anomalous incoming shortwave radiation obtained from J-OFURO2 for each summer. As expected from year-to-year variation at KEO, there were large year-to-year variations southeast of Japan, especially in the Kuroshio Extension region that produced basin-scale anomalous heating in 2004 and 2005 and cooling in 2006. This feature is also clearly seen in CLW data that has higher-resolution and is consistent with results of KEO incoming shortwave radiation (see Figure 5).

[18] As expected from Figure 3, incoming shortwave radiation is affected by TCs. In order to investigate the relationship between TCs and the spatial pattern of incoming shortwave radiation, Figures 6 and 7 show anomalous TC composites of shortwave radiation and CLW for each summer. The anomalous TC composite was calculated as the composite mean of incoming shortwave radiations over TC periods minus the summertime mean over several summers (2004–2006). From Figures 6 and 7, and comparison with Figure 1, incoming shortwave radiation during TC periods is negative near the TC tracks. Since the TC tracks are variable depending on year, the negative anomaly of incoming shortwave radiation area associated with TC is also variable. In 2004 and 2006, the KE region is characterized by negative anomaly of incoming shortwave radiation associated with TC. On the other hand, in 2005, the KE region is characterized by small positive anomaly of incoming shortwave radiations. It can be seen from the comparison between Figures 4 (5) and 6 (7) that the spatial patterns are roughly similar. These findings suggest that basin scale year-to-year variation of summertime incoming shortwave radiation results from year-to-year variation of incoming shortwave radiation associated with routes of TCs.

[19] An influence of TCs on surface wind speed is also expected. In fact, the year-to-year variation of momentum flux at the KEO is similar to the variation of air-sea heat flux (see Table 3). We will discuss the influence of year-to-year variation of momentum flux through the entrainment process later.

3.3. Year-to-Year Variation in Upper Ocean State

[20] In this section, we focus on upper ocean state at the KEO buoy. Also, the relationship between anomalous summertime heat fluxes as shown in section 3.1 and upper ocean state is also investigated.

[21] Figure 8 shows the comparison of the summertime vertical gradients of potential density (color) and temperature (contour) obtained from the KEO buoy upper ocean data in each year. In 2005, vertical gradients of summertime potential density are large and the maximum is found at 20–60 m depth. In contrast, the vertical gradients of summertime potential density in 2004 and 2006 are quite weak, particularly near the surface. The vertical gradients of temperature (contour) show quite similar variations of that of

Figure 6. Spatial distribution of anomalous TC composite mean of incoming shortwave radiation (W/m^2) obtained from J-OFURO2 for each summer in (a) 2004, (b) 2005, and (c) 2006. The anomalous TC composite was calculated as the composite mean of incoming shortwave radiations averaged exclusively over periods with TC minus the summertime mean. Red triangle shows KEO buoy location.
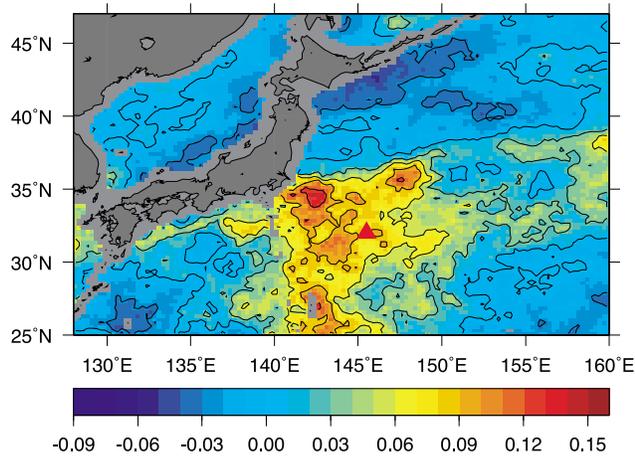
(a) 2004
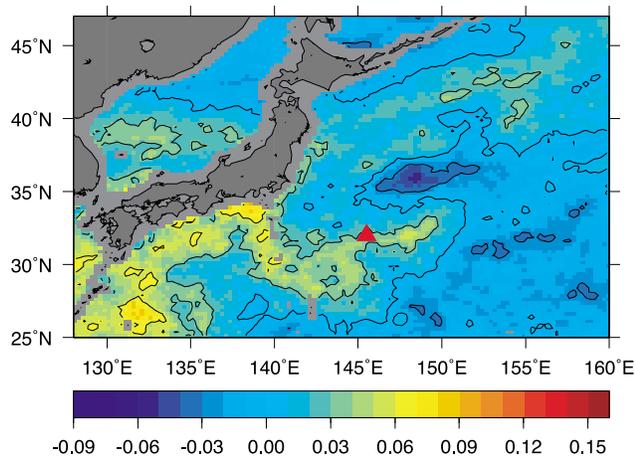
(b) 2005
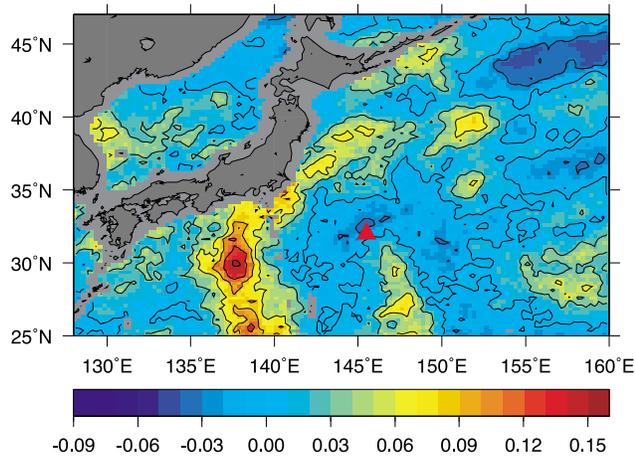
(c) 2006

Figure 7. Same as Figure 6 but for cloud liquid water (mm) obtained from synthesis of multimicrowave radiometers.

potential density (color). From this result, salinity effect on upper ocean stratification is relatively small compared with temperature. To quantify the year-to-year variation of upper ocean stratification, density stratification S is computed as the integrated vertical gradient of potential density over depths listed in Table 5. In summer 2005, anomalous near-surface S (10–100 m) is positive, indicating the upper ocean stratification is strengthened. On the other hand, in summer 2006, anomalous near surface S is negative, indicating that the upper ocean stratification is weakened. This year-to-year variation of near surface S is similar to the surface heat flux variation shown in section 3.1. Surface heat flux plays an important role in the determination of upper ocean stratification.

[22] The year-to-year variations in the deeper S over 100–500 m depth (nominally between the base of the seasonal thermocline and the top of the main thermocline) and the overall S over 10–500 m depth (from near-surface to the top of the thermocline) are evident in Table 5. The year-to-year variation of the overall S is determined by both year-to-year variations in near-surface S and deeper S and the relative importance is roughly comparable. In 2004, both the near-surface and deeper S show negative anomalies. As a result, overall S shows weakest stratification in 2004. On the other hand, in 2005 and 2006, near-surface S and deeper S show opposite signs to each other. In 2005, near-surface and deeper S tend to cancel out for the most part and overall S shows small positive stratification. On the other hand, in 2006, the deeper S is quite large and positive and has a significant role in the large positive value of the overall S anomaly.

[23] Since the Kuroshio Extension region is characterized by oceanic mesoscale eddies (Figure 9), such eddies also have an effect on the formation of upper ocean stratification. In fact, the previous study, which investigated vertical structure of mesoscale eddy, reveals that cyclonic (anticyclonic) eddy was accompanied by intense (mild) stratification in the upper ocean [e.g., *Ebuchi and Hanawa*, 2000]. Intrusion of a cyclonic (anticyclonic) eddy might uplift (depress) thermocline. During 2006, a cyclonic eddy was present at KEO (Figure 9c) and appears to have affected the upper ocean stratification at the KEO. In particular, as shown in Figure 10, altimetric SSHA at KEO and temperature from near surface through depth 500 m have significant covariations.

[24] To confirm the relationship between the oceanic mesoscale eddies and upper ocean stratification, Figure 11 shows scatter diagrams between S and the vertically averaged temperature over the depth from 400 through 500 m as an index of variation of mesoscale eddies. This figure implies that temperature variation associated with eddy activities and the relationship between the eddy and the near-surface stratification is quite variable depending on time. In 2004, there are two different phases that have positive and negative correlations between vertical stratification and eddies. The positive (negative) phase is roughly corresponding to the data in the period of September (July) and intrusion of warm (cold) anomaly. Also, in 2006, the 400–500 m average temperature varies widely from 8°C to 16°C compared with those in 2004 and 2005 and a significant negative correlation (−0.51) is found. This implies that the eddy has significant influence on the intensification of
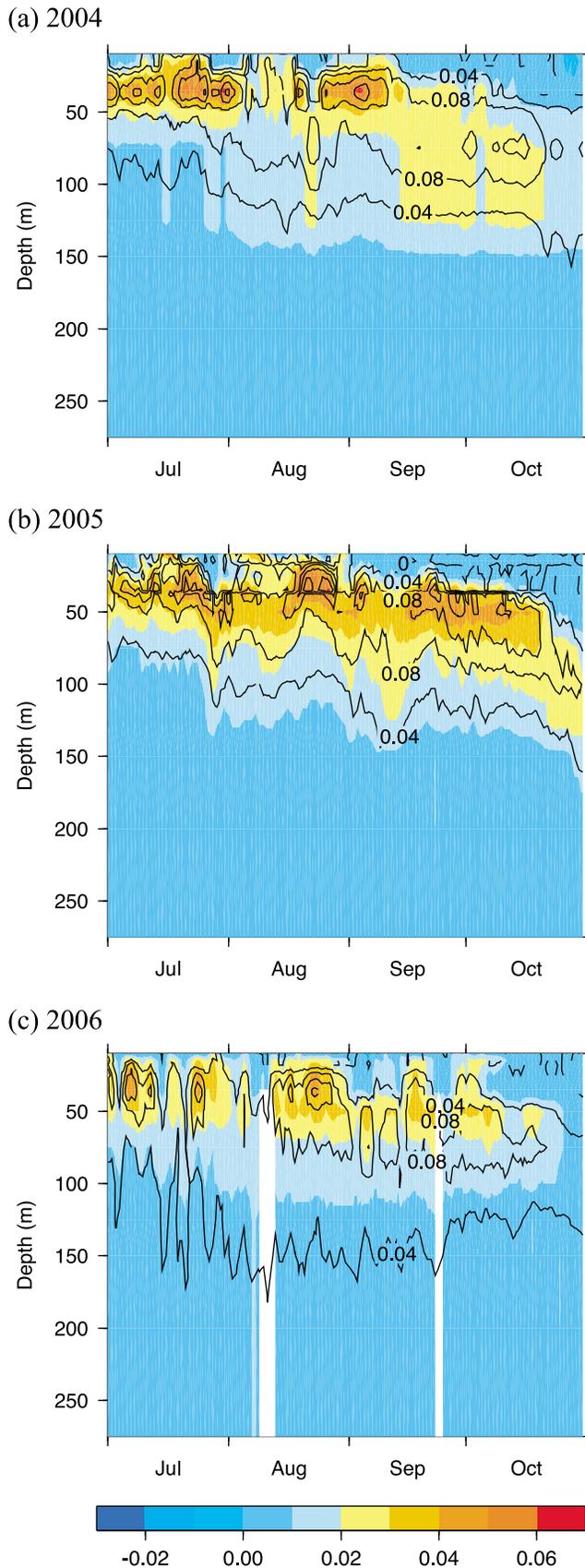
(a) 2004

Table 5. Summertime Average and Anomaly of Density Stratification Defined as Vertical Gradient of Potential Density Integrated Over Depths[a]

Variable	Summertime Average	Anomaly		
		2004	2005	2006
S (10–100 m depth)	2.0	−0.1	0.4	−0.3
S (100–500 m depth)	1.4	−0.2	−0.3	0.5
S (10–500 m depth)	3.3	−0.3	0.1	0.2

[a] S is density stratification. Units in kg/m^3.

near-surface ocean stratification. In contrast to 2006, there is relatively low but significant negative correlation (−0.29) in 2005. This implies that the eddy has a small influence on the upper ocean stratification in 2005 compared with 2006. The eddy also has significant influence on deeper stratification (figure not shown). In particular, in 2006, significant negative correlation between eddy and upper ocean stratification was found not only for near surface S but also deeper S.

[25] These results were also supported by year-to-year variation of eddy kinetic energy obtained from surface current data. Although the KEO has surface current meters, their data return is low. Therefore we used surface vector current data obtained from the satellite-based OSCAR product. The bias, RMS, and correlation coefficients between the KEO and OSCAR data are ∼ −0.14 m/s, 0.38 m/s, and 0.6, respectively. Figure 12 shows time series of the EKE obtained from OSCAR data. EKE indicates large year-to-year variation that is especially strong from March to October 2006. This result suggests that eddies have a large impact on upper ocean state in 2006.

3.4. Influence of Year-to-Year Variation of Lateral, Vertical Fluxes, and Wind Mixing

[26] At the KEO site, south of the Kuroshio Extension jet, mesoscale eddies can be large and therefore lateral fluxes might be important. Also, vertical flux might have a significant impact on summertime mixed layer. Because there are no three-dimensional temperature and current data, the effect of lateral and vertical fluxes on the upper ocean must be estimated indirectly. To do this, first we calculated the heat storage rate (HSR) using temperature data obtained from KEO buoy. The HSR equation can be expressed as follows [*Kako and Kubota*, 2007]:

$$HSR = \frac{\rho_w \cdot C_w}{\Delta t} \int_0^{h_m} (T(z) - T'(z))dz \tag{1}$$

where ρ_w is density of seawater, C_w is the specific heat of water, $T(z)$ is temperature at depth z, h_m is mixed layer depth for the previous time step, Δt is time step (i.e., day), and $T(z) - T'(z)$ is the difference between the temperature

(b) 2005

(c) 2006

Figure 8. Time series of upper ocean state at the KEO buoy for each summer in (a) 2004, (b) 2005, and (c) 2006. Color shade and contour show vertical gradients of potential density (kg/m^3/m) and temperature (°C/m), respectively. Contour interval is 0.02°C/m for temperature.
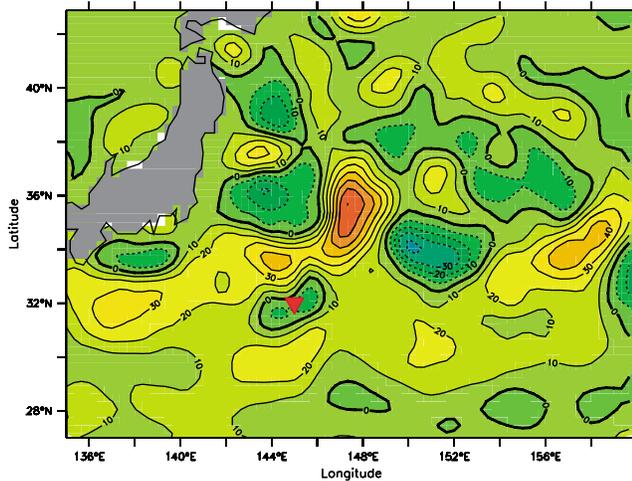
(a) 2004
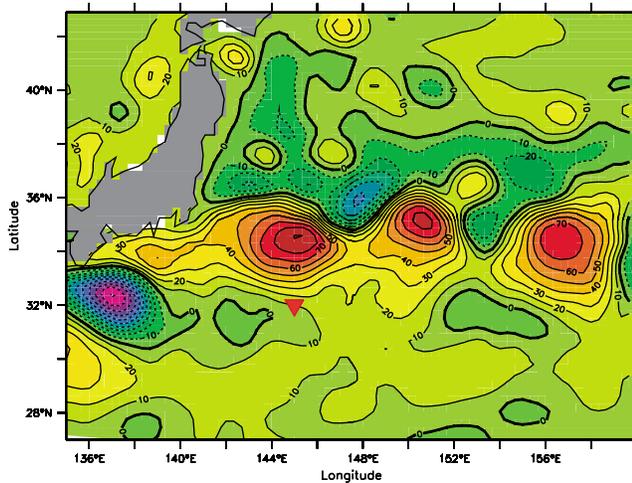
(b) 2005
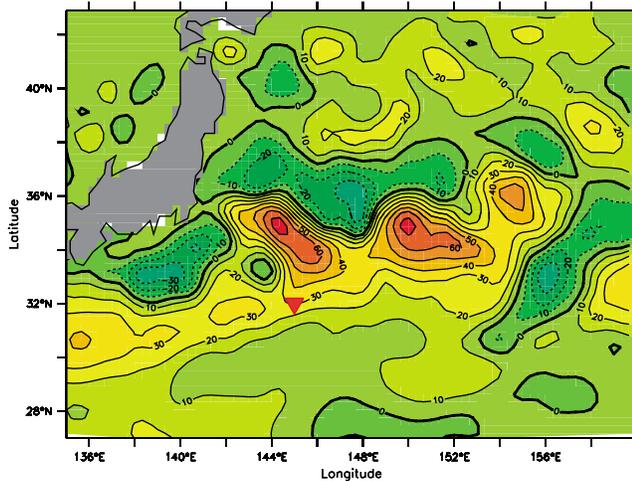
(c) 2006

Figure 9. Spatial distributions of mean SSHA (cm) over the Kuroshio Extension region for each summer in (a) 2004, (b) 2005, and (c) 2006. Red triangle shows KEO buoy location.

of the current and previous time steps. The *HSR* can be also expressed as follows:

$$HSR = \rho_w \cdot C_w \cdot h_m \left(\frac{\partial T_m}{\partial t} \right) = QNET - \rho_w \cdot c_p \cdot w_e \cdot \Delta T + \text{residual}$$

(2)

where w_e is entrainment velocity and ΔT is the temperature difference between mixed layer and the layer below. The first term in the right-hand side of (2) is net heat flux (*QNET*), the second term is entrainment flux (*WE*), and the third term is the residual and includes diffusion and lateral advection terms. We estimated *QNET* and *WE* terms using the KEO buoy data. Then the entrainment velocity w_e was estimated following the method described by *Qiu and Kelly* [1993] (see Appendix A). Finally, we estimated the residual term comparing *HSR*, *QNET*, and *WE* obtained from KEO buoy data. Hereafter we interpret this residual term as the lateral and vertical fluxes term.

[27] Table 6 shows summertime mean and anomaly of *HSR*, *QNET*, *WE*, and residual (which includes lateral and vertical fluxes) terms. The estimated summertime mean residual term is quite large (-38.1 W/m^2) and tends to cool the mixed layer. There is significant year-to-year variation of residual term and its anomaly covaries with *QNET*. In 2004 and 2005, residual fluxes were a warm anomaly while in 2006, the residual term was a cooling anomaly. This result suggests that although the relative influence of surface heat flux and lateral/vertical flux on mixed layer can vary each year, lateral and vertical fluxes have an important role in intensifying year-to-year variation of mixed layer variation.

[28] As well as surface heat flux, wind speed also shows year-to-year variation during 2004–2006. The mixing induced by the year-to-year variation of wind stirring might have significant effect. The mixing effect by wind stirring is included in *WE*. To clarify what physical process is contributing to *WE*, Table 7 shows summertime mean and anomaly of *WE* and its contributing terms: the wind stirring term (*WS*), the surface buoyancy term (*SB*), and the radiation penetration terms (*RP*). On the summertime average, *WS* and *RP* contribute cooling. On the other hand, *SB* contributes to the warming of mixed layer. The balance is variable depending on year. Roughly, anomalies of *SB* and *RP* balance out and that of *WS* contributes *WE* significantly. For example, *WS* contributes to explain about 25% of total anomaly of *HSR* in 2005 (see Table 6).

4. Summary and Discussion

[29] Summertime surface heat flux and upper ocean state in 2004, 2005, and 2006 obtained from the KEO buoy were analyzed to investigate the role of summertime preconditioning on the following winter's mixed layer. Summertime incoming shortwave radiation shows large year-to-year variation and leads to the anomalous summertime heating in 2005 and the anomalous cooling in 2006 (Table 3). The variation of incoming shortwave radiation in summertime was largely related to variations in the TC activity over the Kuroshio Extension region (Figure 3). Analysis of the spatial pattern in the global surface heat flux product, J-OFURO2, also suggested that year-to-year variation of summertime incoming
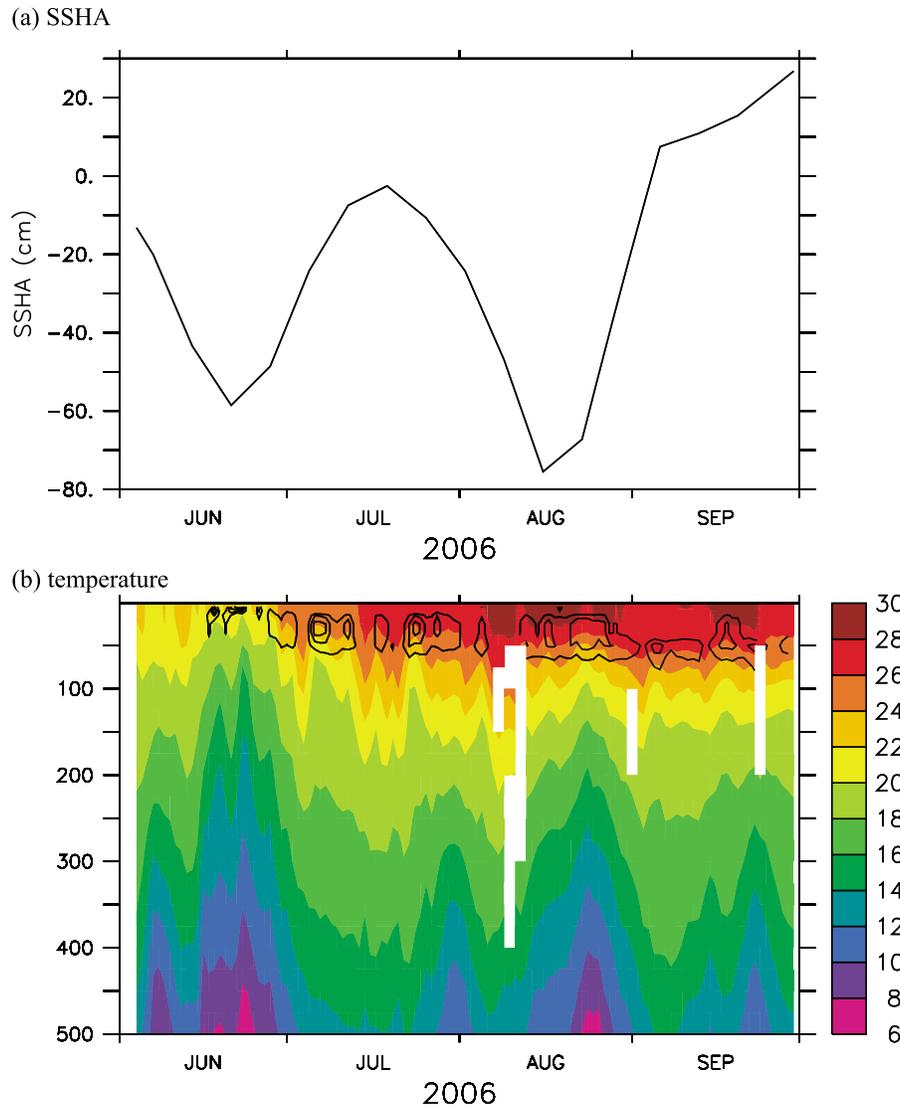
(a) SSHA

(b) temperature

Figure 10. Time series of (a) SSHA and (b) temperature at the KEO buoy from June through September 2006. The strong vertical gradient of potential density (>0.025 kg/m^3/m) was superimposed on temperature time series as contour.

shortwave radiation in the western North Pacific results from year-to-year variation of TC activity. In 2004 and 2006, the KE region is characterized by negative anomaly of incoming shortwave radiation associated with the high TC activity in the vicinity of KEO. On the other hand, in 2005, the typhoons in the KE region were relatively weak and far from KEO. Consequently, summer 2005 is characterized by a weak positive anomaly of incoming shortwave radiations.

[30] Significant year-to-year variations were also found in the summertime vertical gradient of potential density in 2004, 2005, and 2006. The variations of vertical gradients of potential density were caused primarily by temperature variations, as the salinity effect is relatively small. Large vertical gradients were found at 20–60 m depth in summer 2005, while weaker vertical gradients were found in summers 2004 and 2006 (Figure 8). This covariation of surface heat flux and upper ocean state suggests that year-to-year variation of summer-time heat flux induces year-to-year variation of near surface stratification.

[31] The year-to-year variation of vertical density stratification in the relatively deeper region (100–500 m depth) was also found and plays a significant role in determining the overall upper ocean state (Table 5). In particular, in 2005 and 2006, anomalies of near surface stratification and deeper stratification have opposite signs and modulate overall upper ocean state.

[32] The year-to-year variations of mesoscale eddy and lateral and vertical fluxes also have a dominant role on the upper ocean state. The eddy activity indicates significant year-to-year variation that is especially strong in 2006. A cold-core ring was observed in 2006 at the KEO buoy (Figure 9), which appeared to influence both the near surface and deeper density stratifications. The residual lateral and vertical fluxes also have a significant role in determination of upper ocean stratification and can intensify year-to-year variation of mixed layer (Table 6).

[33] The results in the present study are consistent with the results of *Kako and Kubota* [2007], who performed
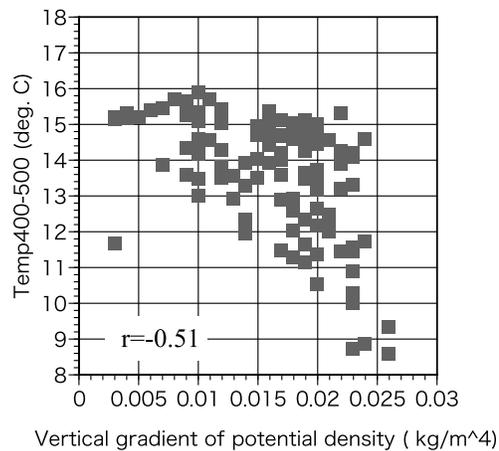
(a) 2004
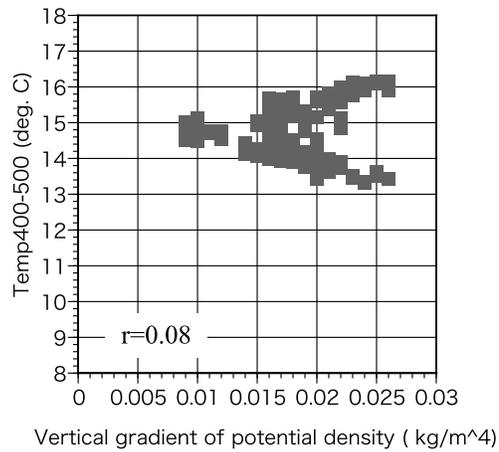
(b) 2005
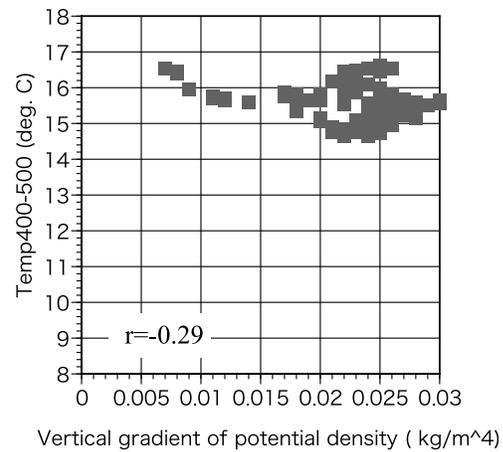
(c) 2006

Figure 11. Scatterplots between surface stratification and temperature averaged over the depth of 400–500 m for each summer in (a) 2004, (b) 2005, and (c) 2006.
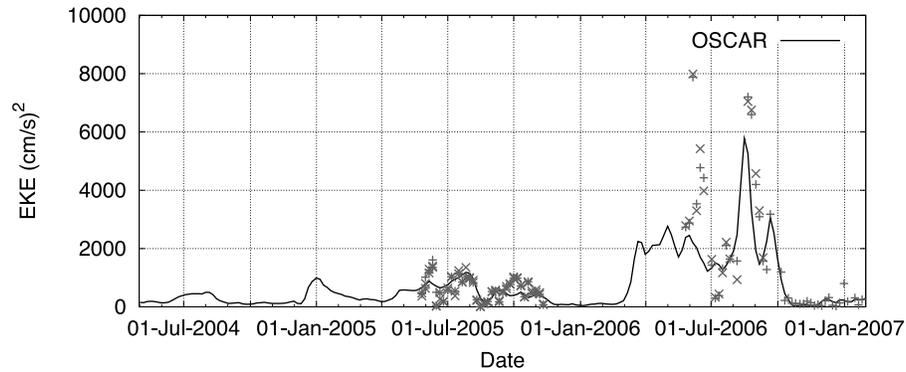
Figure 12. Time series of EKE $(cm/s)^2$ calculated from KEO (point) and OSCAR (line) surface current vector data at the KEO buoy.

numerical experiments using one-dimensional turbulent closure mixed layer model and showed that anomalous surface forcing during summer 2005 caused anomalous stratification in the upper ocean. They also showed the summertime anomalous stratification of the upper ocean in 2005 led to shallower mixed layer in the following winter (i.e., 2005–2006). Our results, that use in situ observations, agree with and confirm their numerical results.

[34] Our results also indicate anomalous cooling in summertime in 2006, which appears to lead to weaker stratification in summertime in 2006 and a deeper mixed layer in the following winter (i.e., 2006–2007). However, the development of wintertime mixed-layer in 2006–2007 is inhibited to less than 200 m of maximum (see Figure 2). This implies that oceanic stratification over a much deeper region also has an impact on the next winter's mixed layer depth (Table 5). Indeed, the large influence of a cyclonic eddy on deeper region was found in 2006. This aspect of our results is consistent with results of *Qiu and Chen* [2006], who demonstrated a relationship between mesoscale eddy activity and density stratification at decadal time scale. Also our results showing the large differences in upper ocean state each year are consistent with changes of the Kuroshio Extension state. The Kuroshio Extension state changed from low eddy activity state in 2002–2004 to a high eddy kinetic energy state in 2005 [*Qiu et al.*, 2007].

[35] While the length of the in situ observational data is only 3 years, our results suggest that the year-to-year variation of summertime surface heat flux and oceanic variations were dominated by variations of TC and mesoscale eddy activity, respectively, and that these anomalous sum-

mertime conditions contribute to the upper ocean stratification, preconditioning the system for the winter mixed layer. This fact suggests that relatively smaller scale air-sea phenomena such as TC and mesoscale eddy can have a major impact on large-scale climate. Further research focusing on the interactions between TCs and the KE is warranted. For such future work and for further investigations of air-sea interaction processes in this dynamic region, continuous and simultaneous observations of air-sea flux and upper ocean state are indispensable.

Appendix A: Calculation of Entrainment Velocity

[36] To estimate entrainment velocity w_e, we follow the method described by *Qiu and Kelly* [1993]:

$$\frac{1}{2}agh_m\Delta Tw_e = m_0u_*^3 + \frac{ag}{\rho_wc_w}\int_{-h_m}^{0}q(z)dz - \frac{agh_m}{2\rho_wc_w}(QNET + q_d)$$
$$- m_c\frac{agh_m}{4\rho_wc_w}(|QNET| - QNET) \qquad (A1)$$

The first term on the right-hand-side denotes the energy source of wind stirring (where $u* = (|MF|/\rho)^2$ is friction velocity for momentum flux (*MF*) and the constant $m_0 = 0.5$ [*Qiu and Kelly*, 1993]). The second term denotes the radiation penetration term (where α is the thermal expansion coefficient $= 2.5 \times 10^{-4}$ /°C and q is the downward radiation flux). The last two terms denote the surface buoyancy term (where q_d is the radiation flux at the base of mixed layer and m_c is the convective efficiency coefficient $= 0.83$ [*Deardorff et al.*, 1969]). When the mixed layer is in the shoaling phase,

Table 6. Summertime Average and Anomaly of Heat Storage Rate, Surface Net Heat Flux, Entrainment Flux, and Residual Lateral and Vertical Fluxes[a]

Term	Summertime Average	Anomaly		
		2004	2005	2006
HSR	−14.5	26.0	29.1	−55.1
QNET	84.4	6.4	16.5	−22.9
WE	−61.0	14.3	1.7	−15.9
Lateral and vertical fluxes	−38.1	5.6	10.4	−16.1

[a]Heat storage rate, HSR, surface net heat flux, QNET, entrainment flux, WE. Units in W/m^2.

Table 7. Summertime Average and Anomaly of the Terms Contributing to the Entrainment Flux[a]

Term	Summertime Average	Anomaly		
		2004	2005	2006
WE	−61.0	14.3	1.7	−15.9
WS	−44.6	6.6	7.6	−14.2
SB	70.2	−16.6	42.3	−25.8
RP	−86.6	24.2	−48.2	24.1

[a]Wind stirring term (WS, $-2m_0u_*^3\rho c_p/agh_m$), the surface buoyancy terms (SB, $(QNET + q_d) + m_c(|QNET| - QNET)/2$) and the radiation penetration terms (RP, $-2\int_{-hm}^{0}q(z)dz/h_m$). Units in W/m^2. See also Appendix A.

the $w_e = 0$ in our estimate. Please note that the energy source from the shear production was not taken into account as well as in the work of *Qiu and Kelly* [1993]. In the HSR equation (2), we estimate the term of *WE* and its contributing terms: the wind stirring term (*WS*), the radiation penetration terms (*RP*), and the surface buoyancy term (*SB*), as follows:

$$WE = WS + RP + SB$$
$$= -2m_0 u_*^3 \rho_w c_p / a g h_m - 2 \int_{-h_m}^{0} q(z) dz / h_m + (QNET + q_d)$$
$$+ m_c (|QNET| - QNET)/2 \tag{A2}$$

References

Bonjean, F., and G. S. E. Lagerloef (2002), Diagnostic model and analysis of the surface currents in the tropical Pacific Ocean, *J. Phys. Oceanogr.*, *32*, 2938–2954, doi:10.1175/1520-0485(2002)032<2938:DMAAOT>2.0.CO;2.

Cronin, M. F., C. Meinig, C. L. Sabine, H. Ichikawa, and H. Tomita (2008), Surface mooring network in the Kuroshio Extension, *IEEE Syst. J.*, *2*, 424–430.

Deardorff, J. W., G. E. Willis, and D. K. Lilly (1969), Laboratory investigation of non-steady penetrative convection, *J. Fluid Mech.*, *35*, 7–35, doi:10.1017/S0022112069000942.

Ebuchi, N., and K. Hanawa (2000), Mesoscale eddies observed by TOLEX-ADCP and TOPEX/POSEIDON altimeter in the Kuroshio recirculation region south of Japan, *J. Oceanogr.*, *56*, 43–57, doi:10.1023/A:1011110507628.

Hosoda, S., T. Ohira, and T. Nakamura (2008), A monthly mean dataset of global oceanic temperature and salinity derived from Argo float observations, *JAMSTEC Rep. Res. Dev.*, *8*, 47–59.

Kako, S., and M. Kubota (2007), Variability of mixed layer depth in Kuroshio/Oyashio Extension region: 2005–2006, *Geophys. Res. Lett.*, *34*, L11612, doi:10.1029/2007GL030362.

Kubota, M., N. Iwabe, M. F. Cronin, and H. Tomita (2008), Surface heat fluxes from the NCEP/NCAR and NCEP/DOE reanalyses at the Kuroshio Extension Observatory buoy site, *J. Geophys. Res.*, *113*, C02009, doi:10.1029/2007JC004338.

Qiu, B., and S. M. Chen (2006), Decadal variability in the formation of the North Pacific Subtropical Mode Water: Oceanic versus atmospheric control, *J. Phys. Oceanogr.*, *36*, 1365–1380, doi:10.1175/JPO2918.1.

Qiu, B., and K. A. Kelly (1993), Upper-ocean heat-balance in the Kuroshio Extension region, *J. Phys. Oceanogr.*, *23*, 2027–2041, doi:10.1175/1520-0485(1993)023<2027:UOHBIT>2.0.CO;2.

Qiu, B., S. M. Chen, and P. Hacker (2007), Effect of mesoscale eddies on subtropical mode water variability from the Kuroshio Extension System Study (KESS), *J. Phys. Oceanogr.*, *37*, 982–1000, doi:10.1175/JPO3097.1.

Suga, T., and K. Hanawa (1995a), The subtropical mode water circulation in the North Pacific, *J. Phys. Oceanogr.*, *25*, 958–970, doi:10.1175/1520-0485(1995)025<0958:TSMWCI>2.0.CO;2.

Suga, T., and K. Hanawa (1995b), Interannual variations of North Pacific subtropical mode water in the 137-degrees-E section, *J. Phys. Oceanogr.*, *25*, 1012–1017, doi:10.1175/1520-0485(1995)025<1012:IVONPS>2.0.CO;2.

Tomita, H., M. Kubota, M. F. Cronin, S. Iwasaki, M. Konda, and H. Ichikawa (2010), An assessment of surface heat fluxes from J-OFURO2 at the KEO/JKEO sites, *J. Geophys. Res.*, *115*, C03018, doi:10.1029/2009JC005545.

M. F. Cronin, NOAA Pacific Marine Environmental Laboratory, Seattle, WA 98115, USA.

S. Kako, Center for Marine Environmental Studies, Ehime University, Matsuyama 790-8577, Japan.

M. Kubota, School of Marine Science and Technology, Tokai University, Shimizu, Shizuoka 424-8601, Japan.

H. Tomita, Research Institute for Global Change, Japan Agency for Marine and Earth Science Technology, Yokosuka, Kanagawa 237-0061, Japan. (tomitah@jamstec.go.jp)